Journal of Catalysis 324 (2015) 59–68

Contents lists available at ScienceDirect

Journal of Catalysis

journal homepage: www.elsevier.com/locate/jcat

Precisely-controlled synthesis of Au@Pd core–shell bimetallic catalyst via atomic layer deposition for selective oxidation of benzyl alcohol

Hengwei Wang, Chunlei Wang, Huan Yan, Hong Yi, Junling Lu *

Department of Chemical Physics, Hefei National Laboratory for Physical Sciences at the Microscale, CAS Key Laboratory of Materials for Energy Conversion, University of Science and Technology of China, Hefei, Anhui 230026, PR China

ARTICLE INFO

Article history:
Received 2 December 2014
Revised 18 January 2015
Accepted 20 January 2015

Keywords:
AuPd bimetallic catalyst
Core–shell structure
Atomic layer deposition
Precisely controlled synthesis
Benzyl alcohol oxidation
Synergistic effect

ABSTRACT

In this study, we report a novel facile strategy for atomically-precise synthesis of supported Au@Pd core–shell bimetallic catalyst via atomic layer deposition (ALD). By choosing a proper deposition condition, we can selectively deposit Pd only on Au nanoparticle surface, but not on SiO_2 support to exclusively form Au@Pd core–shell bimetallic nanoparticles, while avoiding monometallic nanoparticle formation; therein, the Pd shell thickness can be atomically precisely tuned by varying the number of Pd ALD cycles. In solvent-free oxidation of benzyl alcohol, the catalytic activities of the resulted Au@Pd/SiO_2 core–shell bimetallic catalysts showed a clear volcano-like trend with the Pd shell thickness, reaching a maximum at a Pd shell thickness of 0.6–0.8 nm due to the optimized synergistic effect. More importantly, we believe this new strategy of precise synthesis of core–shell structured bimetallic catalyst using ALD can be general to other supported bimetallic catalysts for broad applications.

© 2015 Elsevier Inc. All rights reserved.

1. Introduction

Bimetallic catalysts often show superior catalytic properties compared to those of their parent monometallic counterparts due to the synergistic effect of two components [1–3]. This behavior may mainly originate from the ensemble effect, (particular metal atoms arrangements that are required for facilitating a particular catalytic process) or electronic effect (electronic modification resulting from hetero-nuclear metal–metal bond formation) [1,4]. The catalytic properties of bimetallic catalysts often vary dramatically with their size, structure, and composition. Thus, precisely tuning these factors of bimetallic nanoparticles will make them a new class of materials with enhanced properties for a range of applications.

In particular, core–shell structured bimetallic nanoparticles are currently of enormous interest. In addition to their unique properties, another motivation is to decrease precious metal consumption by coating inexpensive metal cores with a small amount of precious metal while retaining catalytic activity [5,6]. Lots of efforts have been devoted to exploring facile methods of synthesis of core–shell structured bimetallic nanoparticles. The most commonly used synthetic method is the reduction of a second metal onto pre-formed primary metal particles [7–10], while such method often generates undesired monometallic nanoparticles [7,11,12]. Other strategic routes in a more controlled manner were also reported, such as anion coordination protocol [6], sacrificial hydrogen method [13], surface-specific reductants [14], redox transmetalation reactions [15], and controlled simultaneous reduction [16]. Typically, the surface structures, lattice strains, and electronic properties of core–shell bimetallic nanoparticles largely depend on the shell thickness, which thus determines their catalytic performance [8,9,16–18]. Nevertheless, a facile and general strategy to achieve atomically precise control over the shell thickness while avoiding monometallic nanoparticle formation is still missing.

ALD is a variation on chemical vapor deposition in which metals, oxides, and other materials are deposited on surfaces by a sequence of self-limiting reactions [19–22]. In recent years, ALD has demonstrated its great potential in advanced catalysts synthesis beyond its original application in microelectronics [23–28]. Due to its self-limiting features in each deposition cycle, ALD provides a possible method to design and modify catalysts at the nanoscale through precise control over the structure and composition of the underlying support, the catalytic active sites, and the protective layer [29–34]. Very recently, we reported a general strategy of low-temperature selective metal ALD for atomically precise synthesis of supported bimetallic catalysts [34], wherein monometallic nanoparticle formation is avoided by selectively growing a secondary metal on the primary metal nanoparticle but not on

* Corresponding author.
E-mail address: junling@ustc.edu.cn (J. Lu).

http://dx.doi.org/10.1016/j.jcat.2015.01.019
0021-9517/© 2015 Elsevier Inc. All rights reserved.

the support using ALD. Meanwhile, the size, composition, and structure of the bimetallic nanoparticles can be precisely controlled by tailoring the precursor pulse sequences.

However, Au ALD is still currently not applicable due to a lack of a proper Au ALD precursor, even though Au monometallic and Au-based bimetallic catalysts are extremely interesting systems in catalysis [35–37]. For example, AuPd bimetallic catalysts have showed superior catalytic performance in many reactions such as CO oxidation [38,39], direct synthesis of hydrogen peroxide [40,41], direct synthesis of vinyl acetate [42], formic acid decomposition [43,44], and oxidation of carbon–hydrogen bonds [45]. In particular, AuPd bimetallic nanoparticles can remarkably enhance the catalytic activity and product selectivity in primary alcohol oxidations [37,46–56].

Herein we report a novel strategy to precisely synthesize SiO_2 supported Au@Pd core–shell catalysts using a combined wet-chemistry and ALD method: We first synthesized Au/SiO_2 catalysts using the deposition–precipitation (DP) method, then Pd was selectively deposited only on the surface of Au nanoparticles but not on the SiO_2 support to exclusively form uniform Au@Pd core–shell nanoparticles, while avoiding monometallic nanoparticle formation. By varying the number of Pd ALD cycles, the thickness of Pd shell was precisely tuned. Extensive characterizations were carried out to confirm this selective deposition and uniform formation of core–shell structured bimetallic nanoparticles. Finally, we evaluated the catalytic performance of the resulted $Au@Pd/SiO_2$ core–shell bimetallic catalysts using solvent-free aerobic oxidation of benzyl alcohol as a probe reaction, and we found that the catalytic activities showed a clear volcano-like trend as a function of Pd ALD cycles (or Pd shell thickness), wherein a Au@Pd core–shell catalyst with a Pd shell thickness of 0.6–0.8 nm showed a maximum activity due to the optimized synergistic effect *via* both ensemble and electronic promotion.

2. Experimental

2.1. Catalyst synthesis

2.1.1. Au/SiO_2 catalyst

A 1 wt% Au/SiO_2 catalyst was first prepared using DP method [57]. Typically, 1 g $HAuCl_4{\cdot}4H_2O$ (Sinopharm Chemical Reagent Co., Ltd.) was dissolved into 50 ml deionized water to prepare 0.0485 mol L^{-1} $HAuCl_4$ aqueous solution. Next, 1.1 ml $HAuCl_4$ aqueous solution, 1.0 g spherical SiO_2, and 80 ml deionized water were co-added into a three-necked bottle and mixed for 30 min under vigorous stirring at 60 °C, and ammonia was used to adjust the pH value between 9 and 10. Then, the system was continued vigorously stirred for another 12 h. The suspension was then centrifuged and washed with deionized water for several times, and dried at 80 °C overnight. Finally, the resulted sample was calcined at 250 °C under 10% O_2 in He at a flow rate of 20 ml min^{-1} for 4 h to obtain the Au/SiO_2 catalyst. Note that mono-dispersed SiO_2 spheres were synthesized according to the modified Stöber method [58].

2.1.2. Pd/SiO_2 catalyst

A 1 wt% Pd/SiO_2 catalyst was prepared by wet impregnation method [59]. Typically, 52 mg $Pd(acac)_2$ (Sinopharm Chemical Reagent Co., Ltd.) was dissolved into 50 ml acetylacetone to prepare a 1.04 mg ml^{-1} impregnation solution. 30.2 ml Pd solution and 1 g spherical SiO_2 were co-added into a 100 ml flask and stirred at 25 °C for 24 h. The solvent was slowly evaporated under stirring. The obtained solid was dried at 110 °C overnight and further calcined at 500 °C under 10% O_2 in He for 3 h followed by a reduction step at 250 °C under 10% H_2 in Ar for 2 h to obtain the Pd/SiO_2 catalyst (Pd/SiO_2-WI). All flow rates were kept at 20 ml min^{-1} with mass flow controllers.

2.1.3. $Au@Pd/SiO_2$ bimetallic catalysts using selective Pd ALD

Pd ALD was carried out on a viscous flow reactor (GEMSTAR-6™ Benchtop ALD, Arradiance). Ultrahigh purity N_2 (99.999%) was used as carrier gas at a flow rate of 200 ml min^{-1}. Pd ALD was used to selectively deposit Pd only on the Au nanoparticle surface of the Au/SiO_2 catalyst, but not on the SiO_2 support to exclusively form Au@Pd core–shell bimetallic nanoparticles, while avoiding monometallic nanoparticle formation. Such selective Pd ALD process was executed on the as-prepared Au/SiO_2 catalysts at 150 °C, using Pd(II) hexafluoroacetylacetonate ($Pd(hfac)_2$, Sigma–Aldrich, >97%) as the Pd precursor and ultrahigh purity H_2 as reductant [34]. Here the $Pd(hfac)_2$ precursor was contained in a sealed stainless steel bottle at 65 °C to get sufficient vapor pressure, and the inlet lines were heated to 110 °C to avoid any condensation. The timing sequence for selective Pd ALD was 300, 180, 25, and 180 s for $Pd(hfac)_2$ exposure, N_2 purge, H_2 exposure, and N_2 exposure, respectively. A series of Au@Pd bimetallic catalysts were synthesized by different numbers of Pd ALD cycles, which are denoted as $Au@x Pd/SiO_2$ (here x = 1, 3, 5, 8, 10, 15, and 20, representing the number of Pd ALD cycles). In order to further confirm the selective deposition of Pd only on the Au surface, but not on the SiO_2 support, Pd ALD was also carried out on the bare SiO_2 support for different cycles under the same conditions (xc-Pd/SiO_2, here x = 1, 2, and 8) as a control experiment.

2.2. Characterizations

2.2.1. Structure and compositions

Transmission electron microscopy (TEM) measurements were performed on a JEOL-2010 instrument operated at 200 kV to characterize the morphology of Au/SiO_2 and Pd/SiO_2 catalysts, while characterizations of the Au@Pd bimetallic catalysts were more carefully carried out on an aberration-corrected high-angle annular dark-field scanning TEM (HAADF-STEM) instrument at 200 kV (JEOL-2010F, University of Science and Technology of China). Meanwhile, energy-dispersive X-ray (EDX) spectroscopy was also collected on the same equipment. The compositions and loadings of catalysts were analyzed by an inductively coupled plasma-atomic emission spectrometer (ICP-AES); therein, all samples were dissolved in hot aqua regia.

2.2.2. DRIFTS CO chemisorption

The diffuse reflectance infrared Fourier transform spectroscopy (DRIFTS) CO chemisorption measurements were performed on a Nicolet iS10 spectrometer equipped with an MCT detector and a low-temperature reaction chamber (Praying Mantis Harrick). Before DRIFTS measurements, the samples were calcined in 10% O_2 in He and followed by reduction in 10% H_2 in He at 150 °C. After cooling the sample to room temperature under He, a background spectrum was collected. Subsequently, the sample was exposed to 10% CO in He at a flow rate of 20 ml min^{-1} for about 30 min until saturation. Next, the sample was purged with He at a flow rate of 20 ml min^{-1} for another 30 min to remove the gas phase CO and weakly bonded CO on Au surface, and then the DRIFT spectrum was collected with 256 scans at a resolution of 4 cm^{-1}.

2.2.3. UV–vis and XPS studies

The UV–vis spectra were measured on a Shimadzu DUV-3700 spectrophotometer. The X-ray photoelectron spectroscopy (XPS) measurements were taken on a Thermo-VG Scientific Escalab 250 spectrometer equipped with an Al anode (Al Kα = 1486.6 eV). The binding energies were calibrated using the C 1s peak at 284.4 eV as the internal standard [9]. All samples were pretreated in 10%

H_2 in Ar at a flow rate of 20 ml min^{-1} for 1 h at 150 °C before UV–vis and XPS measurements.

2.3. Catalytic performance

Solvent-free aerobic oxidation of benzyl alcohol using molecular O_2 was carried out in a batch-type reactor under mild conditions. 5 ml benzyl alcohol and 20 mg catalyst were added into a 25 ml three-necked glass flask equipped with a reflux condenser. Prior to reaction, the system was first charged with O_2 by bubbling ultrahigh purity O_2 at a flow rate of 15 ml min^{-1} for 20 min to remove air. Under the continuous flow of O_2, the reactor was immersed into a silicon oil bath at 90 °C to initiate the reaction. During the reaction, the mixture was vigorously stirred at a rate of 1250 rpm to exclude any mass transfer limitation [60]. Finally, the reaction products were analyzed using a Shimadzu GC-2014 gas chromatograph equipped with an Rtx-1 capillary column and an auto-injector.

3. Results and discussion

3.1. Morphology of Au/SiO_2 and Pd/SiO_2 catalysts

Au/SiO_2 and Pd/SiO_2 catalysts were first prepared using the DP and impregnation method, respectively. TEM images and corresponding metal particle size distribution histograms show that metal nanoparticles were well dispersed in both Au/SiO_2 and Pd/SiO_2 samples with a rather narrow size distribution within 3–6 nm, and the mean size calculated from TEM images were 4.0 ± 0.6 nm and 4.7 ± 0.8 nm in Au/SiO_2 and Pd/SiO_2, respectively (Fig. 1). ICP-AES measurements showed that the Au loading in the Au/SiO_2 catalyst was 1.01% and the Pd loading in the Pd/SiO_2 catalyst was 0.92%, both close to the calculated values which demonstrate the high efficiencies of DP and impregnation processes.

3.2. Precise synthesis of $Au@Pd/SiO_2$ bimetallic catalysts using selective Pd ALD

Using the strategy of low-temperature selective metal ALD on metals but not on oxide support, we developed recently, selective Pd ALD was performed on the Au/SiO_2 catalyst by alternatively exposing to $Pd(hfac)_2$ and hydrogen at 150 °C [34]. Here, hydrogen was chosen as the reducing regent instead of formaldehyde to further inhibit the growth on the support [34]. Indeed, we observed that there was negligible Pd loading (0.04%, close to the detection limit) even after 8 cycles of Pd ALD on the bare SiO_2 support as shown in Fig. 2a, which strongly indicates that Pd does not nucleate on the SiO_2 support under these conditions due to the inert properties of Si–OH groups, consistent with our previous results [61]. However, the Pd loadings in the $Au@xPd/SiO_2$ samples (x = 1, 3, 5, 8, 10, 15, and 20) considerably increased along with the number of Pd ALD cycles. Therefore, it is obviously that the Pd must be deposited on the surface of Au nanoparticles of the Au/SiO_2 catalyst, but not on the SiO_2 support, demonstrating the advantage of selective Pd ALD method in bimetallic catalyst synthesis. It is noted that the increase of Pd loading showed a slight lower rate in the first several ALD cycles than the one in the following cycles, which could contribute to the increase in the surface area of Au@Pd bimetallic nanoparticles via the particle size growth.

On Au surface, we speculate that the Pd $(hfac)_2$ precursor very likely undergoes a dissociative chemisorption process *via* Eq. (1) by forming Pdhfac* and hfac* surface species (the asterisk

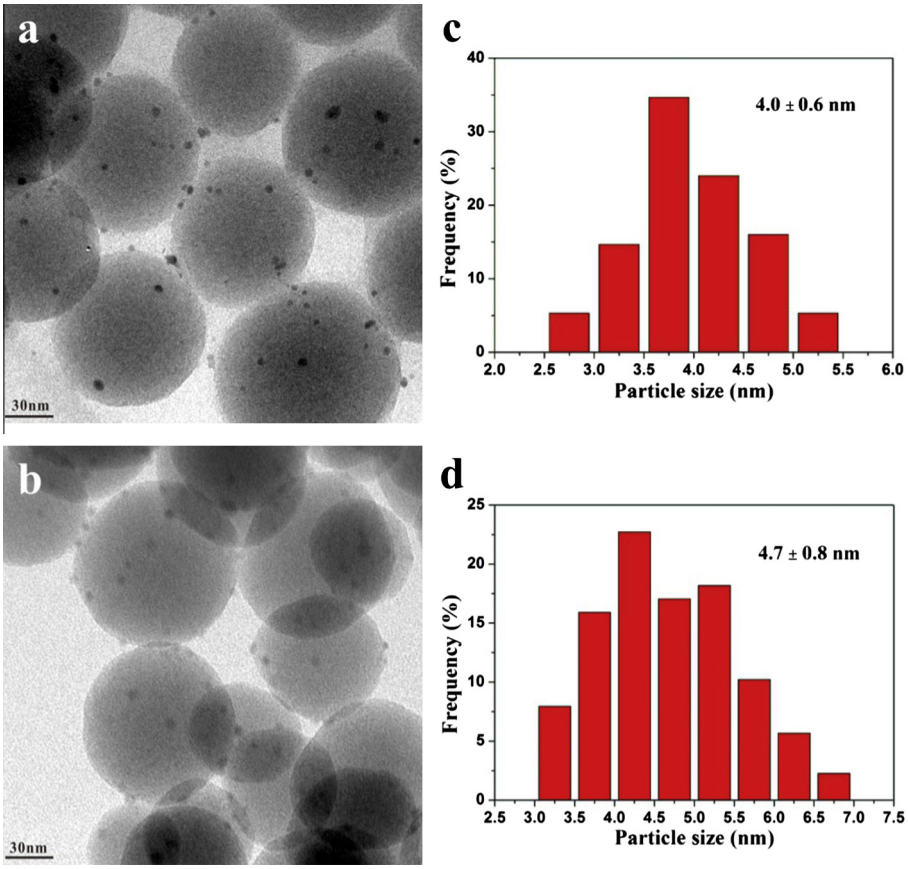

Fig. 1. Representative TEM images of (a) Au/SiO_2, (b) Pd/SiO_2-WI, and (c), (d) the corresponding particle size distributions.

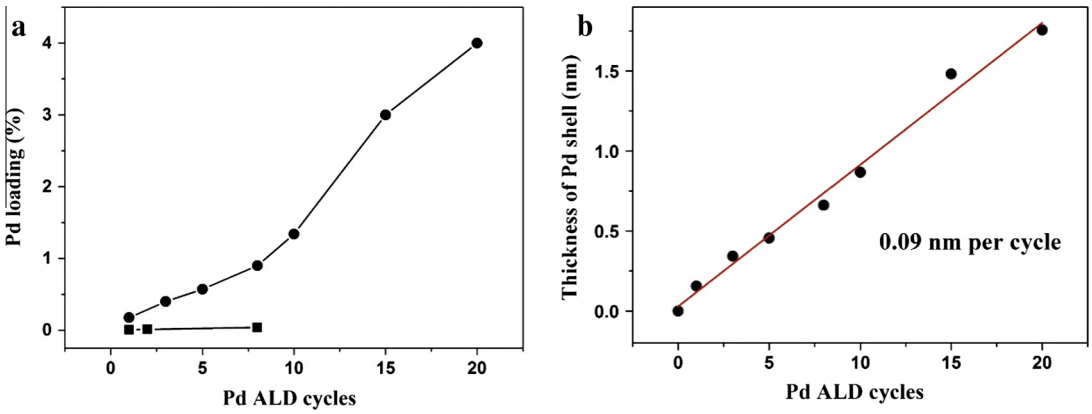

Fig. 2. (a) ICP-AES results of Pd loadings as a function of Pd ALD cycles. Solid circles, Pd ALD on the Au/SiO_2 sample, solid squares, Pd ALD on the SiO_2 support. (b) A linear fitting of the calculated Pd shell thickness as a function of Pd ALD cycles.

designates a surface species, and □ designates a nucleation site), similar to our previous observation of exposing trimethylaluminum on noble metal surfaces [62,63]; next in the hydrogen reduction step, both hfac ligands were removed through Eq. (2) by forming Pd–H* surface species and gaseous Hhfac product. The deposited Pd adatoms on the Au nanoparticles might likely remain isolated from each other or form very small Pd aggregates due to the low surface coverage caused by the steric hindrance of hfac ligand. In the following Pd cycles, the $Pd(hfac)_2$ precursor can either react with the pre-formed Pd–H* species by forming Pd–Pd-hfac* and gaseous Hhfac product (Eq. (3)) or react with the re-exposed Au surface via Eq. (1); hydrogen will again remove all the hfac ligand in the reduction step (Eq. (4)). As a consequence, the amount of Pd on the Au nanoparticles can be precisely controlled by varying the number of ALD cycles.

$$2\square + Pd(hfac)_2(g) \rightarrow Pdhfac^* + hfac^* \quad (1)$$

$$Pdhfac^* + hfac^* + 3/2H_2(g) \rightarrow Pd{-}H^* + \square + 2Hhfac(g) \quad (2)$$

$$Pd{-}H^* + Pd(hfac)_2(g) \rightarrow Pd{-}Pd{-}hfac^* + Hhfac(g) \quad (3)$$

$$Pd{-}Pd{-}hfac^* + H_2(g) \rightarrow Pd{-}Pd{-}H^* + Hhfac(g) \quad (4)$$

Given that low-temperature selective deposition of Pd on Au nanoparticles will likely form Au@Pd core–shell structured bimetallic nanoparticles, we estimated the Pd shell thickness after different Pd ALD cycles using the Au "magic clusters" model [9,64]; therein, a Au nanoparticle was treated as a central Au atom surrounded by closed shells of identical Au atoms. In this model, a 4 nm Au nanoparticle contains seven shells of Au atoms (total number: 1415) [9]; Pd deposited on a 4 nm Au core was approximately considered to form the other shells of the seven-shell Au core. According to the molar ratio of Au/Pd determined by the ICP-AES measurements, this model provides a useful way to estimate the Pd surface coverage in various Au@Pd bimetallic catalysts with different Pd loadings. Given that the thickness of one full monolayer Pd is about 0.227 nm (lattice distance of Pd (1 1 1) planes) [65], thus the thickness of Pd shells in these bimetallic catalysts is obtained. The details of the calculation results are shown in Table 1. To clearly illustrate the trend of the Pd shell thickness as a function of ALD cycles, we further plotted the calculated results as shown in Fig. 2b. It is obviously that the estimated Pd shell thickness rather linearly increased at a rate of 0.09 nm per Pd ALD cycle (or 0.39 Pd monolayer per cycle). Even though one might argue that the variation of size and structures of Au nanoparticle and the contact area between the particles and support would induce uncertainties to the estimations, we believe these approximate results would help us understand the structures of the Au@Pd bimetallic catalysts characterized by other techniques as follows.

3.3. HAADF-STEM characterization and EDX mapping analysis

Aberration-corrected HAADF-STEM measurements were further carried out to investigate the atomic structural information of these bimetallic samples. As shown in Fig. 3a–c, the as-prepared $Au@3Pd/SiO_2$, $Au@8Pd/SiO_2$, and $Au@20Pd/SiO_2$ samples clearly show the gradual particle size growth with Pd ALD cycles, and the growth rate, determined from the slope of the linear fitting of measured mean particle size as a function of Pd ALD cycles, was about 0.14 nm per cycle (Fig. 3d). At higher magnification, all these samples demonstrated a clear Au core–Pd shell structure, where the darker contrast is due to the atomically lighter Pd and the brighter contrast is attributed to the heavier Au (Fig. 3e–g, and i). Here, Au nanoparticles consisted of different orientations wherein the lattice distances of 0.235–0.237 nm and 0.205 nm are assigned to the (1 1 1) and (2 0 0) planes of Au, respectively. The Pd shell in a darker contrast rather uniformly coated on the Au nanoparticles, and the thickness of Pd shells measured from the HAADF-STEM images at different locations of these samples were about 0.33 nm, 0.77 nm, and 1.61 nm for $Au@3Pd/SiO_2$, $Au@8Pd/SiO_2$, and $Au@20Pd/SiO_2$, respectively. The deposition rate, determined from the slope of the linear fitting of measured thickness of Pd shells, as a function of Pd ALD cycles, was 0.08 nm per Pd ALD cycle (or 0.35 Pd monolayer per cycle), as shown in Fig. 3h, which is very close to the expected value, about half of particle size growth rate (0.14 nm per cycle, Fig. 3d). Despite the inevitable errors between the real Au nanoparticles and the "magic cluster" model, or the measuring errors from the STEM images, the deposition rate determined from the STEM images consists very well with the one obtained from the ICP-AES results using the "magic cluster" model, implying the rationality of our estimation about the Pd shell thicknesses. The core–shell structure was further confirmed by the elemental mapping of Au $L\alpha$ and Pd $L\alpha$ on the $Au@8Pd/SiO_2$ sample using EDX (Fig. 3i–l). Even though Au has lower surface energy than Pd [66,67], it is not surprising that we could obtain Au@Pd core–shell nanoparticles by selective Pd ALD at 150 °C, because structural transformation from Au@Pd core–shell to Au–Pd alloy often occurs after heat treatment at about 300 °C or even higher [68–72]. As a consequence, low-temperature selective Pd ALD appears to be possible for synthesis of Au@Pd core–shell bimetallic nanoparticles with precisely tunable Pd shell thickness and compositions by varying the number of Pd ALD cycles.

Table 1
Pd loadings in a series of Au@*x*Pd/SiO_2 bimetallic catalysts with different Pd ALD cycles and the corresponding thicknesses of Pd shells calculated according to the "magic clusters model" based on a 4 nm Au core, which contains 1415 Au atoms.

Pd shell number (n)	Numbers of Pd atoms in shell (n_{atom})[a]	Pd ALD cycles	Pd loading (%)	Pd/Au molar ratio	Pd coverage (ML)	Thickness of Pd shell (nm)
1	642	1	0.17	0.31	0.68	0.16
2	812	3	0.40	0.73	1.5	0.34
3	1002	5	0.57	1.05	2.0	0.46
4	1212	8	0.90	1.65	2.9	0.66
5	1442	10	1.34	2.47	3.8	0.87
6	1692	15	3.0	5.52	6.5	1.48
7	1962	20	4.0	7.36	7.7	1.75
8	2252					

[a] Equation: $n_{atom} = 10 * (n + 7)^2 + 2$.

3.4. DRIFT of CO chemisorption study

The detailed surface structures and compositions of Au@*x*Pd/SiO_2 core–shell bimetallic catalysts were further analyzed by DRIFTS CO chemisorption, because IR studies of CO chemisorption have been widely used to characterize the surface composition of bimetallic nanoparticles [65,68,73–76]. On Au catalyst, CO often weakly bonds to the low-coordinated sites of Au nanoparticles and can be fairly easily purged away with inert gas at room temperature (not shown here) [77]. Thus, the CO chemisorption peaks observed on the Au@Pd bimetallic catalysts after 30 min He purging should attribute to chemisorbed CO on Pd surfaces. Fig. 4 illustrates the DRIFT spectra of CO chemisorption on various bimetallic catalysts recorded at room temperature. On the Au@1Pd/SiO_2 catalyst, two peaks at 2082 and 1980 cm^{-1} were observed, which are assigned to linear and twofold-bridged CO on Pd, respectively. The strong linear CO together with the much weaker twofold-bridged CO strongly indicates that Pd can be majorly isolated Pd adatoms or tiny aggregates [73,76]. With an increase of Pd ALD cycles from 1 to 10, the intensity of linear CO chemisorption band gradually decreased along with a blue shift from 2082 cm^{-1} to about 2093 cm^{-1}, while the twofold-bridged CO developed aggressively. The blue shift of linear CO is due to the increasing dipole–dipole coupling effect, implying the aggregation of Pd atoms [73]. Meanwhile, a new broad shoulder peak at around 1930 cm^{-1} appeared on the Au@8Pd/SiO_2 and Au@10Pd/SiO_2 samples, which is assigned to bridge-bonded CO on Pd(1 1 1) facet, implying the formation of continuous Pd islands or films in (1 1 1) orientation [65,73,75]. This trend in DRIFT spectra of CO chemisorption clearly indicates the gradual evolution of Pd species on Au nanoparticle surfaces while increasing the Pd ALD cycles: from isolated Pd adatoms or very small aggregates to large ensembles, and to continuous islands or films [73,74]. Thus, DRIFT CO chemisorption results provide another strong evidence of precise control over the surface structure of AuPd bimetallic catalysts through the facile low-temperature selective Pd ALD.

3.5. UV–vis and XPS studies

UV–vis and XPS characterizations were employed to further understand the electronic properties of the well-controlled Au@*x*Pd/SiO_2 bimetallic catalysts. As shown in Fig. 5, the UV–vis spectrum of the Au/SiO_2 catalyst showed a characteristic surface plasma resonance (SPR) band centered at 529 nm [8,74,78], while the Pd/SiO_2-WI catalyst does not show any SPR band between 200 and 800 nm. Deposition of Pd onto Au nanoparticles for even one Pd ALD cycle (Au@1Pd/SiO_2) led to significantly decline and broaden the Au SPR band, indicating that the Au surface was covered by Pd to form Au@Pd bimetallic nanoparticles [8,78]. The Au SPR band was gradually obscured while increasing the Pd ALD cycles, implying the gradual thickening of Pd shells, consistent very well with the ICP-AES and STEM results. Note that the Au SPR bands demonstrated a slight blue shift as increasing the Pd ALD cycles, which is contributed to the electron density increase in Au caused by the Pd shells [8,79].

On the other hand, the disturbance of Pd shell 3d electrons by the Au core as a function of the Pd shell thickness was investigated using XPS measurements. As shown in Fig. 6a, the Pd $3d_{3/2}$ and $3d_{5/2}$ binding energies were 340.4 and 335.2 eV on the Pd/SiO_2-WI sample, respectively, which are assigned to zero-valence Pd [9]. Focusing on the Pd $3d_{5/2}$ peak, we observed it was 334.7 eV on the Au@1Pd/SiO_2 sample, and it gradually shifted to higher binding energies as increasing Pd ALD cycles. On the Au@20Pd/SiO_2 sample, the Pd $3d_{5/2}$ binding energy was 335.1 eV very close to the Pd/SiO_2-WI sample [9,65]. The $3d_{5/2}$ binding energy shifts on these bimetallic catalysts from zero-valence Pd (335.2 eV) were further emphasized as a function of Pd ALD cycles as shown in Fig. 6b. It is obvious that the thinner of the Pd shell, the more negative shift of the Pd $3d_{5/2}$ binding energy, strongly indicating the modification of Pd electronic properties by Au tightly depends on the Pd shells thickness [9,74]. The negative shift implies the Pd 3d level draws electrons from Au in the bimetallic system, even though electrons intuitively transfer from Pd to Au, suggested by our UV–vis results, which is due to the higher electronegativity of Au. This phenomenon could be interpreted with the electron transfer model that in a AuPd bimetallic system, Au usually gains s, p electrons and loses d electrons while Pd loses s and p electrons but gains d electrons [4,8,68,80]. Therefore, Pd gaining d electrons from Au explains the negative shift of Pd 3d binding energy in Au@*x*Pd/SiO_2 bimetallic samples. Moreover, this electron transfer model between Au and Pd indicates a stronger interaction of Au–Pd than Au–Au or Pd–Pd, which favors the formation of isolated Pd adatoms on Au at low Pd coverages [4,42,73], consistent with our observation in DRIFT CO chemisorption on Au@1Pd/SiO_2 (Fig. 4). Such electronic interaction between Au and Pd persists on the Au@20cPd/SiO_2 sample, showing a small negative shift (~0.1 eV) of Pd $3d_{5/2}$ binding energy, even though the Pd shell thickness on this sample was about 1.61 nm.

3.6. Catalytic performance

The catalytic performance of monometallic and bimetallic catalysts was evaluated in solvent-free selective oxidation of benzyl alcohol at 90 °C using molecular O_2 as oxidant [60]. As shown in Fig. 7, the Au/SiO_2 catalyst was totally inactive, which is likely due to the large size of the Au particles or the inert property of SiO_2 support [37]. The Pd/SiO_2-WI catalyst also showed a poor activity, and the conversion was only 35% after 6 h reaction, even though the selectivity to benzaldehyde was about 94% [60,65,81,82]. As a control experiment, the 8c-Pd/SiO_2 ALD catalyst was also tested and it did not show any catalytic activity as what we expected, again providing strong evidence that Pd cannot

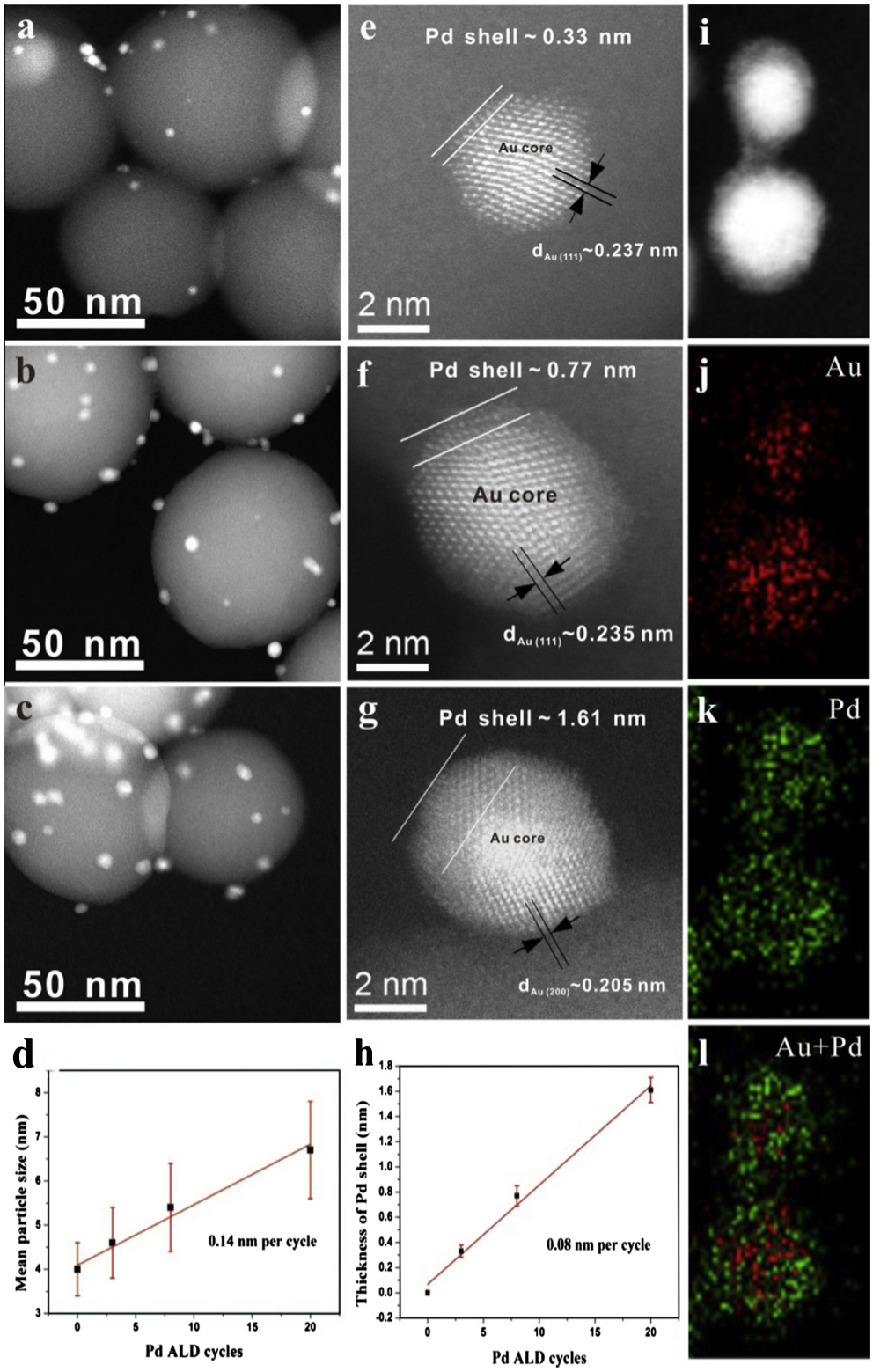

Fig. 3. Aberration-corrected HAADF-STEM images of different bimetallic catalysts at low and high magnifications: (a) and (e) Au@3Pd/SiO_2; (b) and (f) Au@8Pd/SiO_2; (c) and (g) Au@20Pd/SiO_2. (d) The growth of Au@Pd particle size as a function of Pd ALD cycles. (h) The Pd shell thickness as a function of Pd ALD cycles. (i) A lower magnification HAADF-STEM image of Au@8Pd/SiO_2, and corresponding EDX mapping images: (j) Au Lα1 and (k) Pd Lα1 signals, and (l) the reconstructed Au@Pd bimetallic composition image.

deposit on the SiO_2 support under current Pd ALD conditions. On the other hand, remarkable increases of catalytic activities were observed on all the Au@*x*Pd/SiO_2 (*x* = 1, 3, 5, 8, 10, 15, 20) bimetallic catalysts. Among them, high conversion of benzyl alcohol about 90% after 6 h reaction was obtained on Au@8Pd/SiO_2, Au@10Pd/SiO_2, Au@15Pd/SiO_2, and Au@20Pd/SiO_2 catalysts.

Table 2 summarizes the conversion and the product selectivity on all these catalysts after the initial 1 h and 6 h reaction, respec-

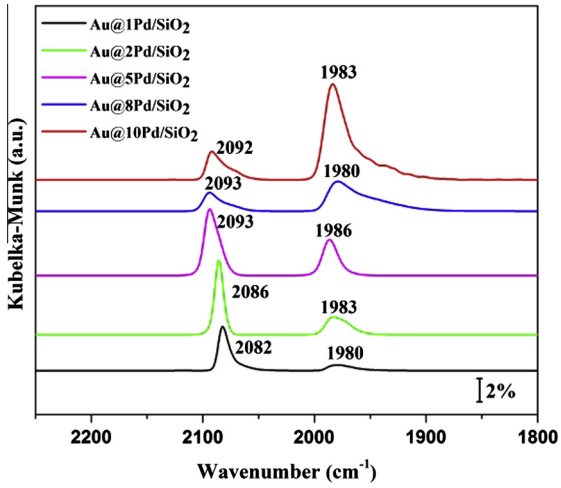

Fig. 4. DRIFT spectra of CO chemisorption at 298 K on various Au@*x*Pd/SiO_2 catalysts at the CO saturation coverage.

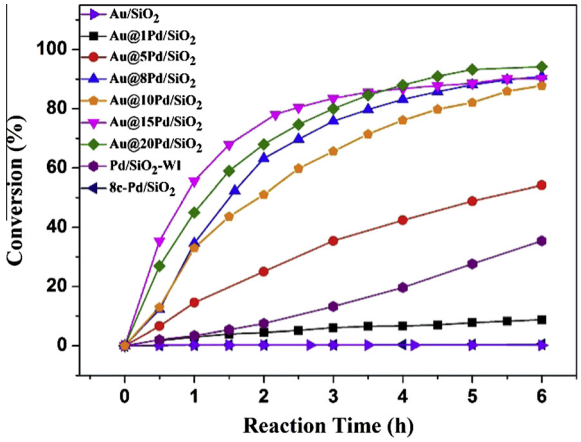

Fig. 7. Conversions of benzyl alcohol versus reaction time over Au/SiO_2, Pd/SiO_2-WI, 8c-Pd/SiO_2, and various Au@*x*Pd/SiO_2 catalysts. Reaction conditions: benzyl alcohol, 5 ml; catalyst, 20 mg; O_2, 15 ml min^{-1}; stirring speed, 1250 rpm; temperature, 90 °C.

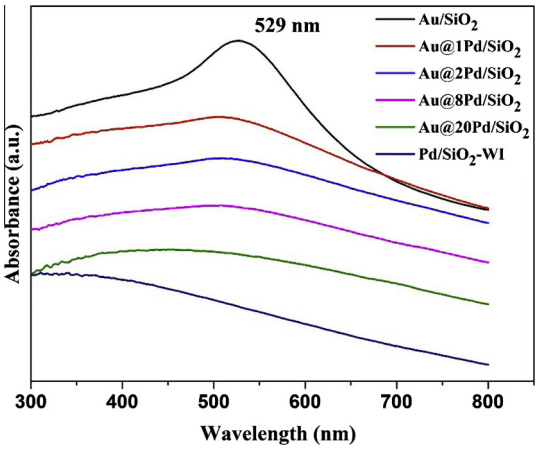

Fig. 5. UV–vis spectra of Au/SiO_2, Pd/SiO_2-WI, and various Au@*x*Pd/SiO_2 catalysts.

tively. After the first 1 h reaction, the benzaldehyde selectivity was rather low and toluene was the main by-product for all the bimetallic catalysts. The benzaldehyde selectivity decreased as increasing Pd ALD cycles, which was only 64% at a conversion of 45% on the Au@20Pd/SiO_2 catalyst, while the toluene selectivity was as high as 35%. Similar trend was also observed in the low conversion range, when we compare the benzaldehyde selectivity at the same conversion. For example, at about 55% conversion, the benzaldehyde selectivity was about 93% and 67% on Au@5Pd/SiO_2 and Au@15Pd/SiO_2, respectively. Such observations are consistent with the previous studies that toluene is generated from the disproportionation of benzyl alcohol via either a hydrogen transfer or an oxygen transfer mediated by surface-enriched Pd over a Pd-rich shell/Au-rich core structure [65]. Nevertheless, the benzaldehyde selectivity all increased to near 90% on all the Au@*x*Pd/SiO_2 bimetallic catalysts as preceding the reaction for 6 h, consistent with the previous studies that the benzaldehyde selectivity is independent of Au:Pd ratio [49,65]. Meanwhile, the toluene formation was significantly inhibited to only a few percent. Corma and coworkers suggested that the Au–H and Pd–H species that formed on supported Au and Pd catalysts are important in the toluene formation [83]. Therefore, we speculate that the accumulation of surface oxygen on the Pd shells with reaction time facilitates the removal of Au–H and Pd–H surface species, thus might be the main reason for the effective inhibition of toluene formation pathway.

To gain the information of the intrinsic reaction rate over the Pd shell thickness, we calculated both the turnover frequency (TOF) and specific activity after 1 h reaction based on the number of surface Pd sites estimated using the "magic cluster" model and the

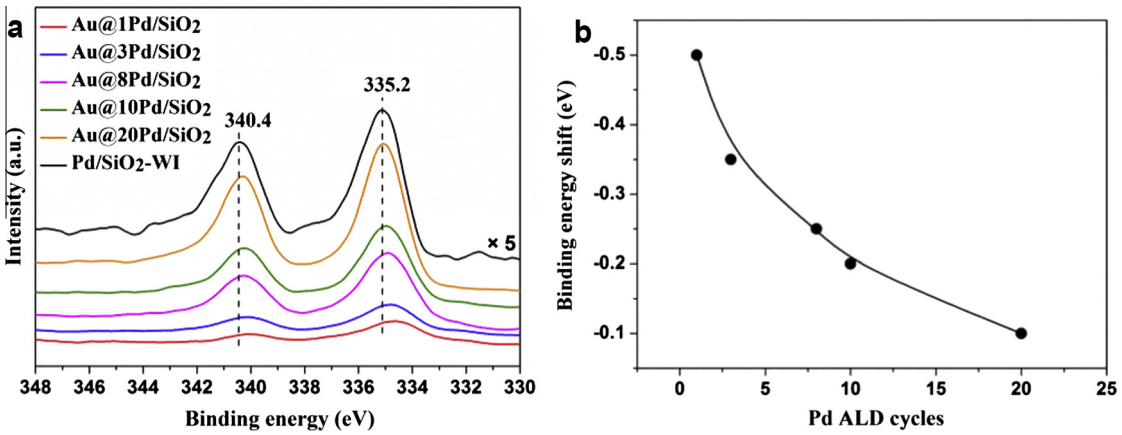

Fig. 6. (a) XPS spectra in the Pd 3d region for a variety of catalysts. Here, the spectrum of Pd/SiO_2-WI sample was amplified by 5 times for a better comparison. (b) Binding energies shift for a variety of bimetallic catalysts compared to the Pd binding energy in the Pd/SiO_2-WI as a function of Pd ALD cycles.

Table 2
Catalytic performance comparisons in solvent-free selective oxidation of benzyl alcohol on series catalysts after 1 h and 6 h reaction. Reaction conditions: benzyl alcohol, 5 ml; catalyst, 20 mg; O_2, 15 ml min^{-1}; stirring speed, 1250 rpm; temperature, 90 °C.

Samples	Time (h)	Conversion (%)	Selectivity (%)			
			Benzaldehyde	Toluene	Benzoic acid	Benzyl benzoate
Au/SiO_2	1	<0.5	NA	NA	NA	NA
	6	<0.5	NA	NA	NA	NA
Pd/SiO_2-WI	1	3.4	93	0.6	2.2	4.7
	6	35	94	0.5	1.9	4.1
8c-Pd/SiO_2	1	<0.5	NA	NA	NA	NA
	6	<0.5	NA	NA	NA	NA
$Au@1Pd/SiO_2$	1	2.6	92	8.5	NA	NA
	6	8.8	91	7.1	0.8	1.0
$Au@5Pd/SiO_2$	1	15	80	18	1.0	1.0
	6	54	93	2.2	2.4	2.0
$Au@8Pd/SiO_2$	1	35	73	26	0.8	0.8
	6	91	87	4.6	4.3	3.7
$Au@10Pd/SiO_2$	1	33	74	24	0.8	1.2
	6	88	91	1	3.2	5.0
$Au@15Pd/SiO_2$	1	55	67	31	0.4	1.8
	6	90	88	5.2	1.5	5.5
$Au@20Pd/SiO_2$	1	45	64	35	0.2	0.8
	6	94	88	7.0	2.2	3.0

total amount of Pd, respectively. Here, we did not take Au into account, since Au is almost inactive and Pd is widely considered as the active sites [37,73]. Interestingly, the histograms of TOF and specific activity both demonstrate a volcano-like trend that they gradually increased as Pd shell thickness (or Pd ALD cycles) and reached maximums at 27,600 h^{-1} and 9800 h^{-1} on the $Au@8Pd/SiO_2$ bimetallic catalyst (Pd shell thickness, ~0.8 nm), respectively; then, they both decreased as further increasing Pd shell thickness (Fig. 8), which is different from the values reported previously, wherein the maximum activity was observed on Au@Pd core–shell catalysts with a Pd shell thickness of one atomic layer [84] and 2.2 nm [56], respectively. However, we noticed the leaching of metal nanoparticles to a certain extent during the recycling tests on the $Au@8Pd/SiO_2$ bimetallic catalyst due to the weak interaction between metal particles and the "inert" SiO_2 support and lack of catalyst stability enhancement by high-temperature pretreatment [37]. Nevertheless, the superior catalytic performance of Au@Pd core–shell bimetallic catalysts over the Au and Pd monometallic catalysts can be addressed to the synergistic effect [2,37,48]. Moreover, the volcano-like trend of catalytic activities as a function of the Pd shell thickness clearly indicates that aerobic oxidation of benzyl alcohol is a structure-sensitive reaction [2,47,65,82]. A similar volcano-like behavior was also observed on the Au–Pd alloy catalysts [53]. However, when $Au@8Pd/SiO_2$ was annealed at 550 °C for 30 min in 10% H_2 in He to form Au–Pd alloy nanoparticles [85] (indicted by the observation of a large decease of CO chemisorption peaks, especially the bridge-bonded CO in the DRIFT spectra, which is not shown here), the specific activity decreased by about 60–70%, even though the TEM measurements showed the AuPd particle size did not change after high-temperature reduction.

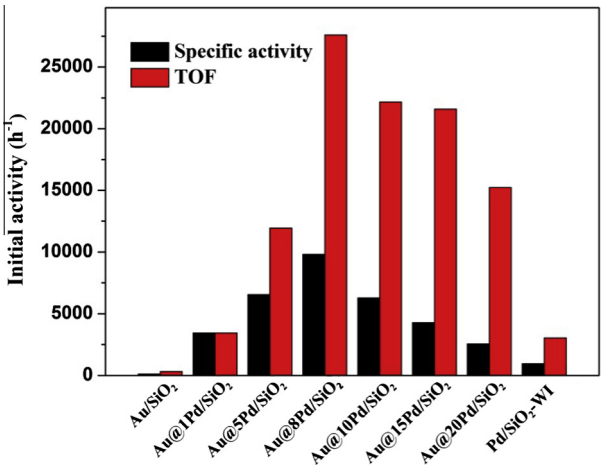

Fig. 8. Initial activities of different catalysts in benzyl alcohol oxidation after 1 h reaction. Specific activity (black column) normalized to the total Pd content; TOF (red column) normalized to the surface Pd content. (For interpretation of the references to color in this figure legend, the reader is referred to the web version of this article.)

A generally accepted mechanism of oxidation of benzyl alcohol over Pd-contained catalysts is first to form the Pd alcoholate intermediate through the interaction of the O–H bond of the alcohol with a Pd site, followed by the β-hydride elimination [2,65,78,86]. Nevertheless, the role of the terrace and low-coordinated (edges and corners) Pd sites is still in the debate. Kaneda et al. [86] suggested that the low-coordinated Pd atoms are the catalytic active site for the formation of Pd alcoholate and the β-hydride elimination, wherein the later step is the rate-limiting step. On the other hand, Baiker et al. [87] proposed that the dehydrogenation of alcohol to carbonyl product could occur virtually on all the surface Pd atoms of Pd/Al_2O_3 catalyst. Wang et al. [82] also observed that TOF depends significantly on the mean size of Pd particles with a maximum at the medium mean particle size (3.6–4.3 nm), thus speculated that benzyl alcohol might first chemisorb on the Pd terrace sites *via* the interaction of the delocalized π-bond of benzene ring and then probably forms Pd alcoholate species, followed by the β-hydride elimination on the nearby edge or corner Pd sites.

In our studies, we observed that isolated Pd adatoms or small aggregates on the $Au@1Pd/SiO_2$ bimetallic catalyst had an apparently lower activity than the continuous Pd islands or shells in (111) orientation on the $Au@Pd/SiO_2$ bimetallic catalyst. This result is in line with the geometric effect suggested by Wang et al. [82] that both terrace and low-coordinated Pd atoms play important role in this reaction, and also explains well the lower activity of Au–Pd alloy compared to Au@Pd core–shell bimetallic nanoparticles, since significantly smaller amount of continuous Pd islands are present on the alloy surface. On the other hand, further increasing Pd shell thicker than 0.8 nm (>8 Pd ALD cycles) resulted in a considerable decrease of TOF and specific activity,

which is probably mainly due to the decline of electronic effects, since the Pd 3d binding energy shift is much less pronounced over the Au@*x*Pd/SiO_2 ($x > 8$) bimetallic catalysts (Fig. 6). As a consequence, the activity appears to be optimized by precisely tuning the Pd shell thickness of Au@Pd core–shell bimetallic catalysts, through the maximization of the synergistic effect *via* both ensemble and electronic promotion.

4. Conclusions

In conclusion, we have successfully demonstrated that low-temperature selective Pd ALD only on Au nanoparticles, but not on the SiO_2 support could be a facile method to exclusively synthesize well-dispersed Au@Pd core–shell bimetallic catalysts supported on SiO_2, while avoiding the formation of monometallic nanoparticles. The thickness of Pd shell can be precisely tuned at a rate of ~0.08 nm per Pd ALD cycle. ICP-AES and aberration-corrected HAADF-STEM measurements were performed to confirm the selective Pd deposition, and the formation of Au@Pd core–shell structured bimetallic catalysts, respectively; DRIFTS CO chemisorption, and UV–vis and XPS measurements were further employed to reveal the evolution of Pd atoms arrangement on Au nanoparticle surface and the electronic properties of the bimetallic nanoparticles as a function of Pd ALD cycles (or Pd shell thickness), respectively. In solvent-free aerobic oxidation of benzyl alcohol, we discovered that the catalytic activities of resulted Au@Pd core–shell bimetallic catalysts showed a clear volcano-like trend as a function of Pd shell thickness, wherein a Au@Pd core–shell catalyst with a Pd shell thickness of 0.6–0.8 nm showed a maximum TOF of 27,600 h^{-1} (or a specific activity of 9800 h^{-1}) due to the synergistic effect *via* both ensemble and electronic promotion. Finally, it is worthy to note that synthesizing core–shell structured bimetallic nanoparticles using a combined wet-chemistry and gas phase ALD method could further extend the application of ALD in catalysis. Moreover, this low-temperature selective metal ALD on the metal particle surface of a monometallic catalyst could be general for other metals and supports and thus opens great opportunities for atomically precise synthesis of various supported bimetallic catalysts with core–shell structures for broad applications.

Conflict of interest

The authors declare no competing financial interest.

Acknowledgments

This work was supported by National Natural Science Foundation of China (21473169), the National Science Foundation for Young Scientists of China (51402283), the Fundamental Research Funds for the Central Universities (WK2060030014), the Recruitment Program of Global Youth Experts, the Scientific Research Foundation for the Returned Overseas Chinese Scholars, and University of Science and Technology of China for the startup funds.

References

[1] F. Maroun, F. Ozanam, O.M. Magnussen, R.J. Behm, Science 293 (2001) 1811–1814.
[2] Z. Guo, B. Liu, Q. Zhang, W. Deng, Y. Wang, Y. Yang, Chem. Soc. Rev. 43 (2014) 3480–3524.
[3] J. Greeley, T.F. Jaramillo, J. Bonde, I.B. Chorkendorff, J.K. Norskov, Nat. Mater. 5 (2006) 909–913.
[4] F. Gao, D.W. Goodman, Chem. Soc. Rev. 41 (2012) 8009–8020.
[5] K. Sasaki, H. Naohara, Y. Cai, Y.M. Choi, P. Liu, M.B. Vukmirovic, J.X. Wang, R.R. Adzic, Angew. Chem. Int. Ed. 49 (2010) 8602–8607.
[6] C.J. Serpell, J. Cookson, D. Ozkaya, P.D. Beer, Nat. Chem. 3 (2011) 478–483.
[7] B. Lim, H. Kobayashi, T. Yu, J.G. Wang, M.J. Kim, Z.Y. Li, M. Rycenga, Y.N. Xia, J. Am. Chem. Soc. 132 (2010) 2506–2507.
[8] A. Sárkány, O. Geszti, G. Sáfrán, Appl. Catal. A: Gen. 350 (2008) 157–163.
[9] M.O. Nutt, K.N. Heck, P. Alvarez, M.S. Wong, Appl. Catal. B: Environ. 69 (2006) 115–125.
[10] I. Srnova-Sloufova, B. Vlckova, Z. Bastl, T.L. Hasslett, Langmuir 20 (2004) 3407–3415.
[11] M. Harada, K. Asakura, N. Toshima, J. Phys. Chem. 97 (1993) 5103–5114.
[12] H. Yu, P.C. Gibbons, K.F. Kelton, W.E. Buhro, J. Am. Chem. Soc. 123 (2001) 9198–9199.
[13] N. Toshima, Y. Shiraishi, A. Shiotsuki, D. Ikenaga, Y. Wang, Eur. Phys. J. D 16 (2001) 209–212.
[14] J. Turkevic, G. Kim, Science 169 (1970) 873.
[15] W.R. Lee, M.G. Kim, J.R. Choi, J.I. Park, S.J. Ko, S.J. Oh, J. Cheon, J. Am. Chem. Soc. 127 (2005) 16090–16097.
[16] A. Sarkany, P. Hargittai, A. Horvath, Top. Catal. 46 (2007) 121–128.
[17] P. Strasser, S. Koh, T. Anniyev, J. Greeley, K. More, C.F. Yu, Z.C. Liu, S. Kaya, D. Nordlund, H. Ogasawara, M.F. Toney, A. Nilsson, Nat. Chem. 2 (2010) 454–460.
[18] S.F. Xie, S.I. Choi, N. Lu, L.T. Roling, J.A. Herron, L. Zhang, J. Park, J.G. Wang, M.J. Kim, Z.X. Xie, M. Mavrikakis, Y.N. Xia, Nano Lett. 14 (2014) 3570–3576.
[19] S.M. George, Chem. Rev. 110 (2010) 111–131.
[20] T. Suntola, J. Hyvarinen, Annu. Rev. Mater. Sci. 15 (1985) 177–195.
[21] R.L. Puurunen, J. Appl. Phys. 97 (2005) 121301.
[22] B.S. Lim, A. Rahtu, R.G. Gordon, Nat. Mater. 2 (2003) 749–754.
[23] J.S. King, A. Wittstock, J. Biener, S.O. Kucheyev, Y.M. Wang, T.F. Baumann, S.K. Giri, A.V. Hamza, M. Baeumer, S.F. Bent, Nano Lett. 8 (2008) 2405–2409.
[24] A.C. Johansson, J.V. Larsen, M.A. Verheijen, K.B. Haugshoj, H.F. Clausen, W.M.M. Kessels, L.H. Christensen, E.V. Thomsen, J. Catal. 311 (2014) 481–486.
[25] H. Feng, J.W. Elam, J.A. Libera, W. Setthapun, P.C. Stair, Chem. Mater. 22 (2010) 3133–3142.
[26] T.D. Gould, A.M. Lubers, B.T. Neltner, J.V. Carrier, A.W. Weimer, J.L. Falconer, J.W. Medlin, J. Catal. 303 (2013) 9–15.
[27] C.P. Canlas, J.L. Lu, N.A. Ray, N.A. Grosso-Giordano, S. Lee, J.W. Elam, R.E. Winans, R.P. Van Duyne, P.C. Stair, J.M. Notestein, Nat. Chem. 4 (2012) 1030–1036.
[28] Y.J. Pagan-Torres, J.M.R. Gallo, D. Wang, H.N. Pham, J.A. Libera, C.L. Marshall, J.W. Elam, A.K. Datye, J.A. Dumesic, ACS Catal. 1 (2011) 1234–1245.
[29] J. Lu, B. Fu, M.C. Kung, G. Xiao, J.W. Elam, H.H. Kung, P.C. Stair, Science 335 (2012) 1205–1208.
[30] J.L. Lu, P.C. Stair, Angew. Chem. Int. Ed. 49 (2010) 2547–2551.
[31] J.L. Lu, J.W. Elam, P.C. Stair, Acc. Chem. Res. 46 (2013) 1806–1815.
[32] A.C. Alba-Rubio, B.J. O'Neill, F.Y. Shi, C. Akatay, C. Canlas, T. Li, R. Winans, J.W. Elam, E.A. Stach, P.M. Voyles, J.A. Dumesic, ACS Catal. 4 (2014) 1554–1557.
[33] T.J. Schwartz, B.J. O'Neill, B.H. Shanks, J.A. Dumesic, ACS Catal. 4 (2014) 2060–2069.
[34] J. Lu, K.B. Low, Y. Lei, J.A. Libera, A. Nicholls, P.C. Stair, J.W. Elam, Nat. Commun. 5 (2014).
[35] M. Haruta, Faraday Discuss. 152 (2011) 11–32.
[36] M. Valden, X. Lai, D.W. Goodman, Science 281 (1998) 1647–1650.
[37] D.I. Enache, J.K. Edwards, P. Landon, B. Solsona-Espriu, A.F. Carley, A.A. Herzing, M. Watanabe, C.J. Kiely, D.W. Knight, G.J. Hutchings, Science 311 (2006) 362–365.
[38] K. Qian, W. Huang, Catal. Today 164 (2011) 320–324.
[39] J. Xu, T. White, P. Li, C.H. He, J.G. Yu, W.K. Yuan, Y.F. Han, J. Am. Chem. Soc. 132 (2010) 10398–10406.
[40] J. Edwards, B. Solsona, P. Landon, A. Carley, A. Herzing, C. Kiely, G. Hutchings, J. Catal. 236 (2005) 69–79.
[41] J.K. Edwards, B. Solsona, P. Landon, A.F. Carley, A. Herzing, M. Watanabe, C.J. Kiely, G.J. Hutchings, J. Mater. Chem. 15 (2005) 4595.
[42] M. Chen, D. Kumar, C.W. Yi, D.W. Goodman, Science 310 (2005) 291–293.
[43] W.Y. Yu, G.M. Mullen, D.W. Flaherty, C.B. Mullins, J. Am. Chem. Soc. 136 (2014) 11070–11078.
[44] Y. Huang, X. Zhou, M. Yin, C. Liu, W. Xing, Chem. Mater. 22 (2010) 5122–5128.
[45] L. Kesavan, R. Tiruvalam, M.H. Ab Rahim, M.I. bin Saiman, D.I. Enache, R.L. Jenkins, N. Dimitratos, J.A. Lopez-Sanchez, S.H. Taylor, D.W. Knight, C.J. Kiely, G.J. Hutchings, Science 331 (2011) 195–199.
[46] W. Hou, N. Dehm, R. Scott, J. Catal. 253 (2008) 22–27.
[47] X. Yang, C. Huang, Z. Fu, H. Song, S. Liao, Y. Su, L. Du, X. Li, Appl. Catal. B: Environ. 140–141 (2013) 419–425.
[48] C.Y. Ma, B.J. Dou, J.J. Li, J. Cheng, Q. Hu, Z.P. Hao, S.Z. Qiao, Appl. Catal. B: Environ. 92 (2009) 202–208.
[49] A. Villa, N. Janjic, P. Spontoni, D. Wang, D.S. Su, L. Prati, Appl. Catal. A: Gen. 364 (2009) 221–228.
[50] Y. Chen, H. Lim, Q. Tang, Y. Gao, T. Sun, Q. Yan, Y. Yang, Appl. Catal. A: Gen. 380 (2010) 55–65.
[51] M. Sankar, N. Dimitratos, P.J. Miedziak, P.P. Wells, C.J. Kiely, G.J. Hutchings, Chem. Soc. Rev. 41 (2012) 8099–8139.
[52] R.C. Tiruvalam, J.C. Pritchard, N. Dimitratos, J.A. Lopez-Sanchez, J.K. Edwards, A.F. Carley, G.J. Hutchings, C.J. Kiely, Faraday Discuss. 152 (2011) 63–86.
[53] J. Pritchard, L. Kesavan, M. Piccinini, Q. He, R. Tiruvalam, N. Dimitratos, J.A. Lopez-Sanchez, A.F. Carley, J.K. Edwards, C.J. Kiely, G.J. Hutchings, Langmuir 26 (2010) 16568–16577.
[54] S. Meenakshisundaram, E. Nowicka, P.J. Miedziak, G.L. Brett, R.L. Jenkins, N. Dimitratos, S.H. Taylor, D.W. Knight, D. Bethell, G.J. Hutchings, Faraday Discuss. 145 (2010) 341–356.
[55] N. Dimitratos, J.A. Lopez-Sanchez, J.M. Anthonykutty, G. Brett, A.F. Carley, R.C. Tiruvalam, A.A. Herzing, C.J. Kiely, D.W. Knight, G.J. Hutchings, Phys. Chem. Chem. Phys. 11 (2009) 4952–4961.

[56] A.M. Henning, J. Watt, P.J. Miedziak, S. Cheong, M. Santonastaso, M.H. Song, Y. Takeda, A.I. Kirkland, S.H. Taylor, R.D. Tilley, Angew. Chem. Int. Ed. 52 (2013) 1477–1480.
[57] K. Qian, L.F. Luo, H.Z. Bao, Q. Hua, Z.Q. Jiang, W.X. Huang, Catal. Sci. Technol. 3 (2013) 679–687.
[58] E. Bourgeat-Lami, J. Lang, J. Colloid Interface Sci. 210 (1999) 281–289.
[59] B. Li, H. Li, W.-Z. Weng, Q. Zhang, C.-J. Huang, H.-L. Wan, Fuel 103 (2013) 1032–1038.
[60] D.I. Enache, D. Barker, J.K. Edwards, S.H. Taylor, D.W. Knight, A.F. Carley, G.J. Hutchings, Catal. Today 122 (2007) 407–411.
[61] J. Lu, P.C. Stair, Langmuir 26 (2010) 16486–16495.
[62] J. Lu, B. Liu, J.P. Greeley, Z.X. Feng, J.A. Libera, Y. Lei, M.J. Bedzyk, P.C. Stair, J.W. Elam, Chem. Mater. 24 (2012) 2047–2055.
[63] J. Lu, L. Bin, N.P. Guisinger, P.C. Stair, J.P. Greeley, J.W. Elam, Chem. Mater. 26 (2014) 6752–6761.
[64] L.N. Lewis, Chem. Rev. 93 (1993) 2693–2730.
[65] Y. Chen, H. Wang, C.-J. Liu, Z. Zeng, H. Zhang, C. Zhou, X. Jia, Y. Yang, J. Catal. 289 (2012) 105–117.
[66] A. Jablonski, S.H. Overbury, G.A. Somorjai, Surf. Sci. 65 (1977) 578–592.
[67] L.Z. Mezey, J. Giber, Surf. Sci. 117 (1982) 220–231.
[68] C.W. Yi, K. Luo, T. Wei, D.W. Goodman, J. Phys. Chem. B 109 (2005) 18535–18540.
[69] T. Nakagawa, H. Nitani, S. Tanabe, K. Okitsu, S. Seino, Y. Mizukoshi, T.A. Yamamoto, Ultrason. Sonochem. 12 (2005) 249–254.
[70] Y. Ding, F.R. Fan, Z.Q. Tian, Z.L. Wang, J. Am. Chem. Soc. 132 (2010) 12480–12486.
[71] D. Jana, A. Dandapat, G. De, J. Phys. Chem. C 113 (2009) 9101–9107.
[72] S.J. Mejia-Rosales, C. Fernandez-Navarro, E. Perez-Tijerina, J.M. Montejano-Carrizales, M. Jose-Yacaman, J. Phys. Chem. B 110 (2006) 12884–12889.
[73] L. Zhang, A. Wang, J.T. Miller, X. Liu, X. Yang, W. Wang, L. Li, Y. Huang, C.-Y. Mou, T. Zhang, ACS Catal. 4 (2014) 1546–1553.
[74] A. Wang, X.Y. Liu, C.-Y. Mou, T. Zhang, J. Catal. 308 (2013) 258–271.
[75] T. Lear, R. Marshall, J.A. Lopez-Sanchez, S.D. Jackson, T.M. Klapotke, M. Baumer, G. Rupprechter, H.J. Freund, D. Lennon, J. Chem. Phys. 123 (2005) 174706.
[76] N.E. Kolli, L. Delannoy, C. Louis, J. Catal. 297 (2013) 79–92.
[77] J.D. Grunwaldt, M. Maciejewski, O.S. Becker, P. Fabrizioli, A. Baiker, J. Catal. 186 (1999) 458–469.
[78] W. Zhou, J.Y. Lee, Electrochem. Commun. 9 (2007) 1725–1729.
[79] A.V. Gaikwad, P. Verschuren, E. Eiser, G. Rothenberg, J. Phys. Chem. B 110 (2006) 17437–17443.
[80] J.A. Rodriguez, Surf. Sci. Rep. 24 (1996) 225–287.
[81] T. Mallat, A. Baiker, Chem. Rev. 104 (2004) 3037–3058.
[82] F. Li, Q. Zhang, Y. Wang, Appl. Catal. A: Gen. 334 (2008) 217–226.
[83] A. Abad, C. Almela, A. Corma, H. Garcia, Chem. Commun. (2006) 3178–3180
[84] T.A.G. Silva, E. Teixeira-Neto, N. Lopez, L.M. Rossi, Sci. Rep. 4 (2014) 5766.
[85] X. Wei, X.F. Yang, A.Q. Wang, L. Li, X.Y. Liu, T. Zhang, C.Y. Mou, J. Li, J. Phys. Chem. C 116 (2012) 6222–6232.
[86] K. Mori, T. Hara, T. Mizugaki, K. Ebitani, K. Kaneda, J. Am. Chem. Soc. 126 (2004) 10657–10666.
[87] D. Ferri, C. Mondelli, F. Krumeich, A. Baiker, J. Phys. Chem. B 110 (2006) 22982–22986.